Journal of Electronics, Electromedical Engineering, and Medical Informatics
Homepage: jeeemi.org; Vol. 7, No. 3, July 2025, pp: 597-610 e-ISSN: 2656-8632
RESEARCH ARTICLE OPEN ACCESS

Computational Analysis of Medical Image Generation Using Generative Adversarial Networks (GANs)

Shrina Patel, and Ashwin Makwana

U & P U Patel Department of Computer Engineering, C S Patel Institute of Technology, Charotar University of Science and Technology, Changa-Gujarat, India

Corresponding author: Shrina Patel. (e-mail: shrinapatel310@yahoo.com)

Email Author(s): Dr. Ashwin Makwana (e-mail: ashwinmakwana.ce@charusat.ac.in)

Abstract **The limited availability of diverse, high-quality medical images constitutes a significant obstacle to training reliable deep-learning models that can be used in clinical settings. The traditional methods used for data augmentation generate inadequate medical photos that result in poor model performance and a low rate of successful generalization. This research studies the effectiveness of DCGAN cGAN CycleGAN and SRGAN GAN architectures through performance testing in five essential medical imaging datasets, including Diabetic Retinopathy, Pneumonia and Brain Tumor and Skin Cancer and Leukemia. The main achievement of this research was to perform an extensive evaluation of these GAN models through three key metrics: generation results, training loss metrics, and computational resource utilization. DCGAN generated stable high-quality synthetic images, whereas its generator produced losses from 0.59 (Pneumonia) to 6.24 (Skin Cancer), and its discriminator output losses between 0.29 and 6.25. CycleGAN showed the best convergence potential for Diabetic Retinopathy with generator and discriminator losses of 2.403 and 2.02 and Leukemia with losses at 3.325 and 3.129. The SRGAN network produced high-definition images at a generator loss of 6.253 and discriminator loss of 6.119 for the Skin Cancer dataset. Still, it failed to maintain crucial medical characteristics in grayscale images. GCN exhibited stable performance across all loss metrics and datasets. The DCGAN model required the lowest computing resources for 4 to 7 hours, using 0.9M and 1.4M parameters. The framework of SRGAN consumed between 7 and 10 hours and needed 1.7M to 2.3M parameters for its operation, and CycleGAN required identical computational resources. DCGAN was determined as the ideal model for synthetic medical image generation since it presented an optimal combination of quality output and resource efficiency. The research indicates that using DCGAN-generated images to increase medical datasets serves as a solution for boosting AI-based diagnostic system capabilities within healthcare.**

Keywords Generative adversarial networks (GANs), Medical imaging, Data augmentation, Image synthesis, Deep learning.

1. Introduction

Generative Adversarial Networks (GANs) have extended their modern approaches to medical image generation and augmentation to solve fundamental problems of data limitation and imbalance in medical datasets [1,2]. The driving force behind this work's development is that the accuracy level in diagnosing diseases through deep learning models is comparatively low, and almost all of them need labelled data for their training [3,4]. Obtaining a large amount of data part, particularly in retinopathy and the classification of X-ray pneumonia, is a slow, expensive and, in many cases, impossible process because of the ethical issues involved in using people's images [5,6]. Some basic data augmentation techniques like flipping, rotating, and scaling do not serve the augmented authentic medical images well or enhance the model's ability to generalize the results effectively. Hence, the requirement for higher-level augmentation methods that can produce multiple valuable medical images while retaining diagnostic characteristics increases [7,8]. However, as we can see, there are a lot of problems with the existing approaches for image generation tasks using GANs. The main issue with

Manuscript received February 8, 2024; Accepted April 25, 2025; date of publication May 8, 2025
Digital Object Identifier (**DOI**): https://doi.org/10.35882/jeeemi.v7i3.784

basic GANs is that they do not converge during training or offer poor-quality, unrealistic images. In addition, the generated images may not reflect the necessary architecture and attributes for medical diagnosis [9,10].

For instance, GANs with small or imbalanced training data are more likely to converge to the mode collapse, a scenario whereby the network synthesizes images that are identical or are derivable from another image, which is detrimental when trying to augment the dataset's variety or heterogeneity [11,12]. Further, the generated medical images have some artefacts or unrealistic attributes that pose challenges in clinical use. This GAN architecture is shown on Fig.1. involves two networks: the Generator Network, which transforms D-dimensional noise into synthetic data, and the Discriminator Network, which classifies data as fake or real. Both networks compete, improving over time through adversarial training [13,14,15].

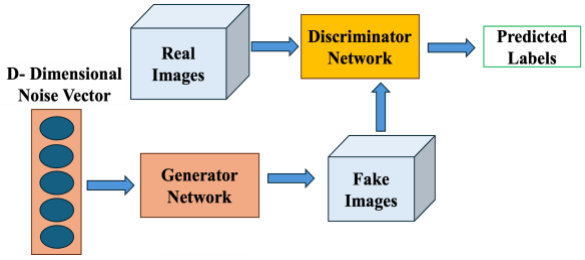

Fig. 1. Architecture of GAN [1]

This paper addresses these limitations by leveraging advanced GAN architectures such as Deep Convolutional GAN (DC-GAN) [2,7,9,19], Conditional Generative Adversarial Networks (cGAN) [6,14,15], CycleGAN [3,13,17], and Super-Resolution GAN (SR-GAN) [10,11,12]. DC-GAN has demonstrated its ability to generate high-quality images using convolutional neural networks, making it ideal for applications like X-ray pneumonia image generation. Cycle-GAN [3,13,17], known for its capability to learn transformations between two domains without paired examples, offers a powerful approach for medical image-to-image translation, such as converting retinal fundus images to segmented vessel maps for retinopathy analysis. SR-GAN, designed for super-resolution tasks, enhances the resolution of medical images, which is particularly useful in improving the clarity and diagnostic quality of low-resolution X-ray and retinal images.

The primary objective of this study is to develop a comprehensive framework for generating synthetic medical images using GANs architectures. By focusing on datasets such as Diabetic Retinopathy, Pneumonia, Brain Tumor, Skin Cancer, and Leukemia Cancer datasets, this research aims to create high-quality synthetic images that improve the performance of deep learning models in diagnostic tasks. The aim is to overcome the limitations of small, imbalanced datasets and produce diverse, high-resolution medical images to enhance AI-driven medical diagnostics' accuracy, robustness, and reliability.

2. Literature Study

Integrating advanced generative models into medical imaging continues to revolutionize the field by addressing challenges such as data scarcity and low-quality images. Wang et al. [1] introduced a self-improving generative foundation model for synthetic medical image generation, showing its applicability in diverse clinical scenarios. Kumar et al. [2] proposed a deep learning-based encryption scheme for medical images using DCGAN and virtual planet domains, enhancing privacy and security in medical image sharing while maintaining the integrity of the photos. Chen et al. [3] presented Cycle-GAN, an improved CycleGAN for liver medical image generation, which outperformed existing models regarding realism and clinical applicability for liver disease detection. Ali et al. [4] offered a comprehensive overview of recent advancements in applying GANs for medical image processing, detailing their effectiveness in synthetic image generation, segmentation, and diagnosis. Sherwani and Gopalakrishnan [5] provided a systematic literature review of deep learning techniques for synthetic medical image generation, focusing on their contributions to radiotherapy applications and the role of GANs in enhancing the precision of treatment planning. These studies demonstrate the substantial impact of generative models on medical imaging, with applications spanning encryption, data augmentation, and disease diagnosis. The utility of GANs in medical image synthesis continues to expand, offering promising results in various domains, including segmentation and disease diagnosis.

Hamghalam and Simpson [6] utilized conditional GANs for medical image synthesis, explicitly focusing on brain tumor segmentation, where their model demonstrated significant improvements in tumor delineation. Akhil et al. [7] applied DCGANs for synthesizing chest X-ray images, proving that GAN-based models could effectively generate realistic medical images for training classifiers and enhancing diagnostic capabilities. Zakaria et al. [8] developed Medical-DCGAN, a deep convolutional GAN tailored for medical imaging tasks, showing its potential to generate high-quality medical images for various applications. Shah et al. [9] explored the reliability of deep learning for breast cancer diagnosis by synthesizing mammograms using DCGANs,

Manuscript received February 8, 2024; Accepted April 25, 2025; date of publication May 8, 2025
Digital Object Identifier (**DOI**): https://doi.org/10.35882/jeeemi.v7i3.784

emphasizing the importance of synthetic data in training robust diagnostic models. Varshitha et al. [10] explored the use of SRGAN for high-quality medical image reconstruction, enhancing the resolution of medical images, which is crucial for accurate diagnosis and treatment planning. These papers highlight the ongoing developments in the field, with GANs and their variants proving effective in generating synthetic medical images that support various diagnostic applications.

The recent advancements in GAN-based medical image synthesis are underscored by their growing application in clinical and diagnostic contexts. Madhav et al. [11] applied SRGANs for the super-resolution of medical images, enhancing their clarity and diagnostic accuracy, particularly in areas like radiology. Nandal et al. [12] utilized ESRGAN (Enhanced Super-Resolution GAN) for the super-resolution of medical images, demonstrating its ability to generate high-resolution images that improve the quality of analysis and interpretation in medical settings. Heng et al. [13] proposed HLSNC-GAN, a model combining hinge loss and switchable normalization in CycleGAN to generate high-quality medical images with improved structure preservation, highlighting its use in disease detection and imaging applications. Jha and Iima [14] employed CycleGAN for CT to MRI image translation, a critical task in cross-modality medical imaging that allows clinicians to gain more comprehensive insights from different imaging modalities. Afnaan et al. [15] introduced a hybrid deep learning framework for bidirectional medical image synthesis, enhancing the capability to translate between different medical image types and further expanding the application of GANs in clinical diagnostics. These studies reflect the increasing sophistication of GAN models, which are becoming indispensable tools for enhancing medical image quality and enabling more accurate clinical decisions.

The application of generative models in medical imaging continues to evolve, with newer approaches focusing on improving image synthesis, segmentation, and diagnostic accuracy. Raad et al. [16] proposed a conditional generative learning approach for medical image imputation, demonstrating its effectiveness in recovering missing or corrupted regions in clinical scans, thereby enhancing diagnostic reliability and downstream analysis. Wang et al. [17] introduced CycleSGAN, a cycle-consistent and semantics-preserving generative adversarial network for unpaired MR-to-CT image synthesis, which effectively handled cross-modality image translation, thus facilitating better interoperability between MR and CT images in clinical settings. Akbar et al. [18] critically assessed the limitations of diffusion models for synthesizing medical photos, comparing them with GANs, and demonstrated that GANs are superior in preventing memorization of images, particularly for complex tasks such as MRI and X-ray synthesis. Devi and Kumar [19] applied DCGAN for diabetic retinopathy (DR) image synthesis and leveraged transfer learning for DR classification, showing promising results in augmenting the dataset for DR detection, which is crucial for early diagnosis. Mamo et al. [20] delivers an extensive review of GAN development in medical imaging which discusses applications, difficulties and prospective avenues for healthcare diagnostic progression. Friedrich et al. [21] researched deep generative models applied to 3D medical image synthesis and reviewed architectural progress with difficulties in multiple modality volumetric data generation. Fard et al. [22] investigated the development of machine learning applications which synthesize interictal SPECT images by combining MRI and PET scans for better neurological disorder diagnosis capabilities. The review article by Islam et al. [23] studied GANs in medical imaging from various perspectives while evaluating their possible applications and describing technical obstacles to clinician uptake. According to Sindhura et al. [24], deep learning techniques and GANs present substantial transformative power for medical image analytics because they lead to better detection of tumors and aid disease monitoring alongside improving source data quantity. The clinical usefulness of deep learning was established when Kermany et al. [25] built an image-driven diagnostic system which detected many treatable diseases, showing the substantial impact on healthcare effectiveness. According to the findings presented in these papers, the sophistication of GANs and deep generative models in medical imaging continues to advance. Medical practitioners use these papers to tackle fundamental tasks, including image synthesis, segmentation, and classification, while improving diagnosis precision. The field of 3D image generation, together with multimodal data translation, shows recent increases in popularity. The research methods yield exceptional results for cases with restricted or unbalanced datasets. The research illustrates how Artificial Intelligence changes medical care practices and improves diagnostic procedures for healthcare providers.

3. Methodology

Fig. 2. illustrates the process of medical image generation using various types of Generative Adversarial Networks (GANs). Medical datasets are first used to train different GAN architectures, including DCGAN, cGAN, CycleGAN, and SRGAN.

Manuscript received February 8, 2024; Accepted April 25, 2025; date of publication May 8, 2025
Digital Object Identifier (**DOI**): https://doi.org/10.35882/jeeemi.v7i3.784

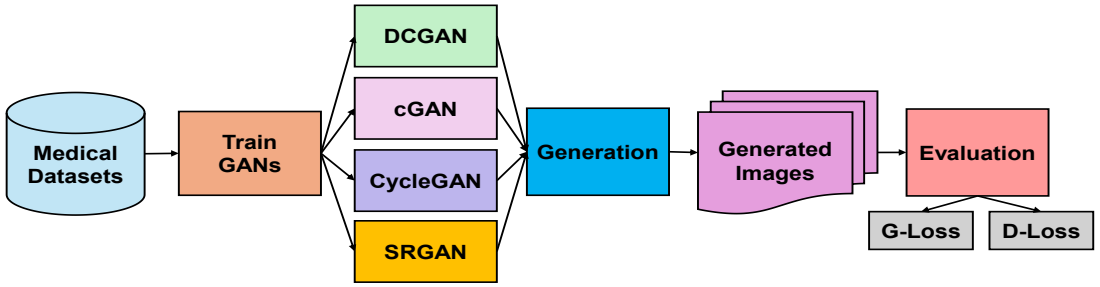

Fig. 2. Methodology Flow

A. Dataset

Table.1 describe the different medical dataset and its size of images and categories of image.

Table 1 Dataset Description

Dataset	Description	Size	Categories
Diabetic Retinopathy [19,27]	Retinal images for detecting diabetic retinopathy (DR)	6993 images	0: No DR, 1: Mild DR, 2: Moderate DR, 3: Severe DR, 4: Proliferative DR
Pneumonia [26]	X-ray images	5,863 images	Pneumonia, Normal
Brain Tumor [28]	MRI images of human brains.	2053 images	Tumors, Normal
Skin Cancer [29]	Dermoscopic images of skin moles.	3297 images	Benign, Malignant
Leukemia Cancer [30]	Leukemia cancer	2940 images	Benign, Early, Pre

B. GANs (Generative Adversarial Networks) [1,3]

GANs consist of two neural networks: a generator and a discriminator, which are trained simultaneously. The generator creates fake data resembling real data distribution, while the discriminator distinguishes between real and generated data. The process is a minimax game, where the generator aims to fool the discriminator, and the discriminator improves his ability to differentiate between real and fake data. The generator, G(z), takes a random input z (usually from a uniform or Gaussian distribution) and generates data x_fake = G(z). The discriminator D(x) outputs the probability that the input is from the real data distribution x_real, aiming to maximize the corre(1ct classification of real versus fake data. The optimization problem for GANs is represented by the following as Eq. (1) [1]:

$$min_G max_D V(D,G) = E_{\{x_{real} \sim p_{data(x)}\}}[log\ D(x)] + E_{\{z \sim p_{z(z)}\}}\left[log\left(1 - D(G(z))\right)\right] \quad (1)$$

Here, $p\_data(x)$ is the real data distribution, and $p\_z(z)$ is the noise distribution. The generator learns to minimize this objective while the discriminator maximizes it, leading to the adversarial dynamic that defines GANs.

C. DC-GAN (Deep Convolutional GAN) [2,7,9,19]

DC-GANs use convolutional layers instead of fully connected layers in the generator and discriminator, making them more suitable for image generation tasks. The generator architecture typically uses a series of transposed convolutional layers (also known as deconvolution layers) to up sample noise into an image, while the discriminator uses regular convolutional layers to classify images as real or fake. The generator starts with a latent vector z ∈ R^d which is projected into a high-dimensional space and then sampled through layers of transposed convolutionsas Eq. (2) [2]:

$$x_{fake} = G(z) = deconv_1\left(deconv_2\left(\ldots\left(deconv_n(z)\right)\right)\right) \quad (2)$$

The discriminator takes an input image and processes it through convolutional layers: $D(x) = \sigma(conv_1(conv_2(\ldots(conv_n(x)))))$, where σ represents a sigmoid activation function that outputs a probability. Key innovations in DC-GANs include replacing pooling layers with stride convolutions and using batch normalization to stabilize training. The architecture enables GANs to generate high-quality images and converge faster than traditional fully connected GANs.

D. cGAN [6,14,15]

Manuscript received February 8, 2024; Accepted April 25, 2025; date of publication May 8, 2025
Digital Object Identifier (**DOI**): https://doi.org/10.35882/jeeemi.v7i3.784

cGAN (Conditional Generative Adversarial Network) is a variant of the traditional GAN designed for tasks where additional information or labels are available to guide the generation process. cGAN introduces a conditional input to the generator G and the discriminator D, where the generator produces data samples conditioned on the input, and the discriminator attempts to distinguish between real and generated samples, also conditioned on the same input. The goal is to learn a mapping G(z, c), where z is random noise and c is a condition (e.g., class label), to generate realistic samples based on the given condition. The discriminator D(x, c) evaluates whether the generated data G(z, c) is real or fake, conditioned on c. The objective function for the cGAN is given by Eq. (3) [6]:

$$L\_\{cGAN\}(G,D) = E\_\{x \sim p\_\{data\}(x)\}[log\ D(x,c)] + E\_\{z \sim p\_z(z)\}[log(1 - D(G(z,c),c))] \quad (3)$$

This structure allows cGAN to generate samples that are not only realistic but also consistent with the conditioning information.

E. Cycle-GAN [3,13,17]

Cycle-GAN is a type of GAN designed for image-to-image translation tasks where paired data (e.g., matching images from two domains) are not available. The goal is to learn mappings between two domains, $X\ and\ Y$, such that an image $x \in X$ can be translated to domain Y (and vice versa) without paired samples. Cycle-GAN introduces two generators, G_{XY} (which maps images from domain X to domain Y) and G_{YX} (which maps images from domain Y to domain X), along with two discriminators, D_X and D_y, which evaluate whether images belong to their respective domains. The innovation of Cycle-GAN lies in the cycle consistency loss, which ensures that if an image is transformed from domain X to domain Y and then back to domain X, it should return to the original image. The cycle consistency loss is defined as Eq. (4) [17]:

$$L_{cyc(G_{XY},G_{YX})} = E_{\{x \sim p_{X(x)}\}}\left[\left|\left|G_{YX(G_{XY(x)})} - x\right|\right|_1\right] + E_{\{y \sim p_{Y(y)}\}}\left[\left|\left|G_{XY\left(G_{YX(y)}\right)} - y\right|\right|_1\right] \quad (4)$$

This ensures that the learned transformations are reversible and maintains the structural integrity of the input images.

F. SR-GAN (Super-Resolution GAN) [10,11,12]

SR-GAN is a GAN designed for image super-resolution, i.e., converting low-resolution images into high-resolution versions. The generator in SR-GAN creates high-resolution images from low-resolution inputs, while the discriminator tries to distinguish between real high-resolution images and the generated ones. The generator employs a series of convolutional and up-sampling layers to predict a high-resolution image from a low-resolution input. The loss function includes both pixel-wise differences and perceptual loss, which measures the discrepancy in high-level feature representations between the real and generated images. The overall objective function for SR-GAN is a combination of adversarial loss and content loss as Eq. (5) [12]:

$$L_{SR} - GAN\ \ L_{adv} + \lambda\, L_{content}, \quad (5)$$

where $L_{adv}$is the adversarial loss that encourages the generator to produce images indistinguishable from real high-resolution images, and $L_{content}$ is the content loss, often based on the perceptual features extracted from a pre-trained deep network like VGG.

G. Parameters

1. Generator Loss [16,17]

The generator's objective is to fool the discriminator into classifying its generated data as real. In standard GANs, the generator loss is derived from the minimax game as Eq. (6) [16]:

$$L_G = -E_{\{z \sim p_{z(z)}\}}\left[log\ D\left(G(z)\right)\right] \quad (6)$$

This loss encourages the generator to produce samples that the discriminator classifies as real (i.e., D(G(z)) → 1). An alternative form of generator loss, called the "non-saturating" loss, is often used in practice to avoid vanishing gradients as Eq. (7) [16]:

$$L_G = E_{\{z \sim p_{z(z)}\}}\left[log\ \left(1 - D\left(G(z)\right)\right)\right] \quad (7)$$

This loss ensures that the gradients do not diminish too quickly, enabling more stable training. In some variations like Wasserstein GAN (WGAN), the generator loss is modified to minimize the Earth Mover's Distance (EMD), improving convergence as Eq. (8) [17]:

$$L_G = -E_{\{z \sim p_{z(z)}\}}\left[D\left(G(z)\right)\right] \quad (8)$$

This encourages the generator to create data that minimizes the Wasserstein distance between the real and generated data distributions.

Manuscript received February 8, 2024; Accepted April 25, 2025; date of publication May 8, 2025
Digital Object Identifier (**DOI**): https://doi.org/10.35882/jeeemi.v7i3.784

2. Discriminator Loss [16,17]

The discriminator's goal is to correctly classify real data as real and generated data as fake. The discriminator loss for a standard GAN as Eq. (9) [17]:

$$L_D = -E_{\{x_{real} \sim p_{data(x)}\}}[log\ D(x_{real})] - E_{\{z \sim p_{z(z)}\}}\left[log\left(1 - D\left(G(z)\right)\right)\right] \quad (9)$$

This loss maximizes the discriminator's ability to differentiate between real and fake data. The first term encourages the discriminator to classify real data correctly, while the second term penalizes it for classifying generated data as real. In WGAN, the discriminator (called the critic) uses a different loss to approximate the Wasserstein distance as Eq. (10) [17]:

$$L_D = -E_{\{x_{real} \sim p_{data(x)}\}}[D(x_{real})] + E_{\{z \sim p_{z(z)}\}}[D(G(z))] \quad (10)$$

This ensures a more stable training process by avoiding the issues of vanishing gradients and mode collapse commonly seen in traditional GANs.

4. Results

Google Colab, with a T4 GPU, provides an efficient environment for implementing and experimenting with advanced deep learning algorithms such as DCGAN, cGAN, CycleGAN, and SRGAN. The platform offers free access to powerful GPUs, enabling the rapid training of generative models. DCGAN, cGAN CycleGAN, and SRGAN were implemented to explore various image generation and transformation tasks for this research. During training, key parameters such as Generator Loss (Error) and Discriminator Loss (Error) were computed to evaluate the performance of each model. During training, hyperparameters selected a batch size of 64, a learning rate of 0.0002, and 5000 epochs. The Adam optimizer was employed to stabilize GAN training effectively.

The figure illustrates the progression of generated diabetic retinopathy images over epochs 1 to 5000. In DCGAN (Fig. 3(a)), early images are noisy and structurally weak, but by epoch 3000, blurry retina-like features begin to emerge, showing gradual convergence with basic vascular patterns. cGAN (Fig. 3(b)), early images are noisy and structurally weak, but by epoch 3000, blurry retina-like features begin to emerge, showing gradual convergence with basic vascular patterns. CycleGAN (Fig. 3(c)) starts with repetitive textures due to untrained generators but improves significantly after epoch 3000, successfully learning domain-specific transformations without needing paired data. SRGAN (Fig. 3(d)) initially produces low-quality patches but gradually enhances fine details and contrast, thanks to perceptual loss, resulting in sharper and more realistic pathological features by epoch 5000. Overall, SRGAN shows superior detail reconstruction, CycleGAN excels in style translation, and DCGAN provides steady but slower improvement in feature generation.

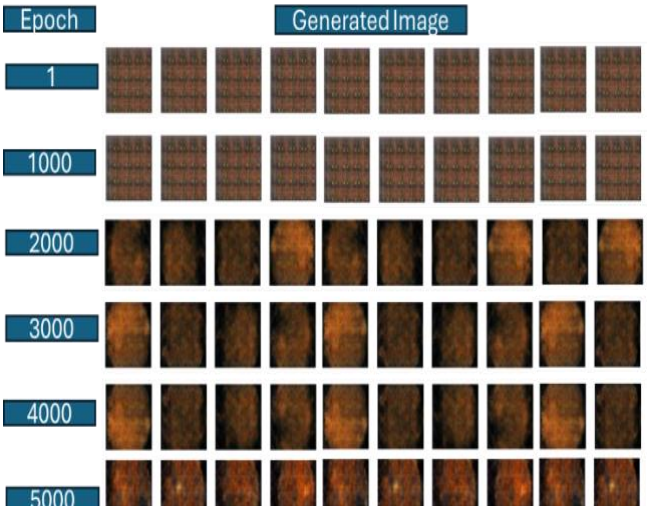

(a)

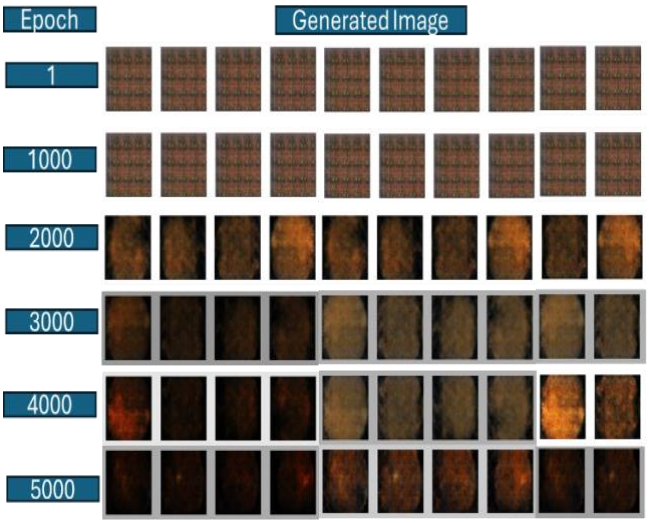

(a)

Manuscript received February 8, 2024; Accepted April 25, 2025; date of publication May 8, 2025
Digital Object Identifier (**DOI**): https://doi.org/10.35882/jeeemi.v7i3.784

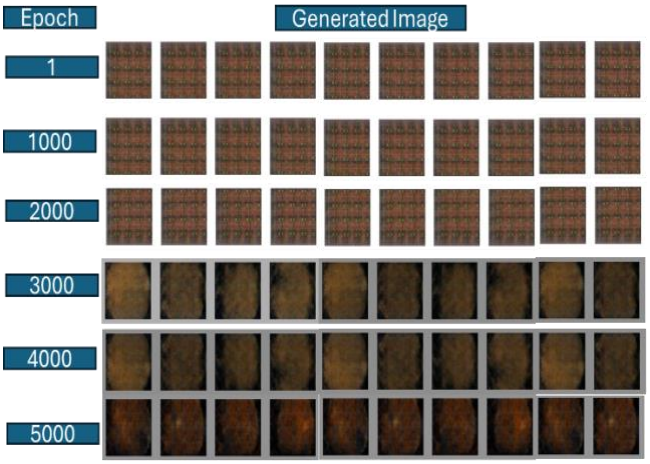

(c)

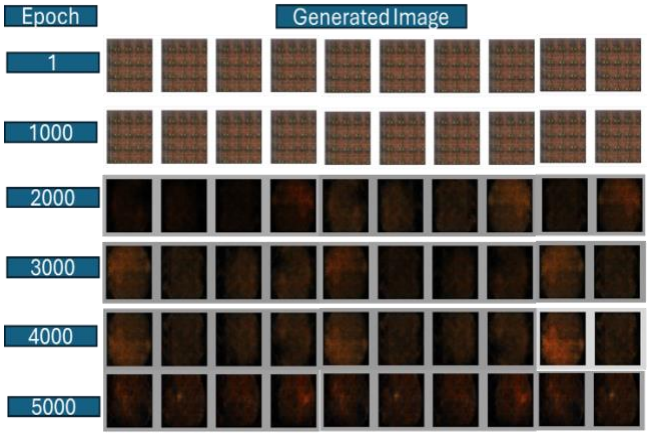

(b)

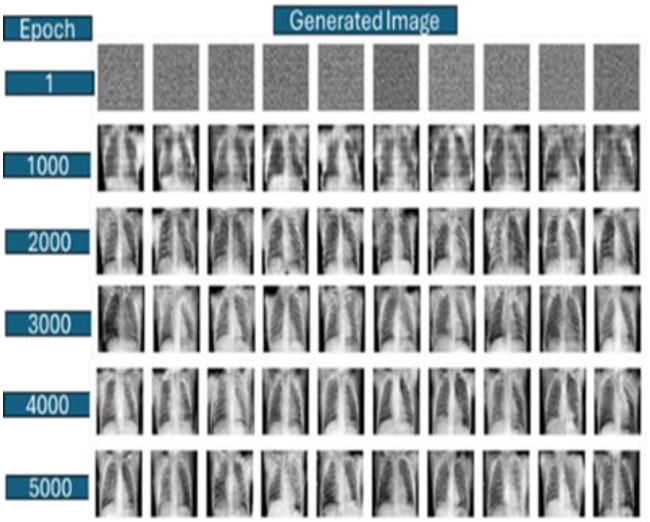

(a)

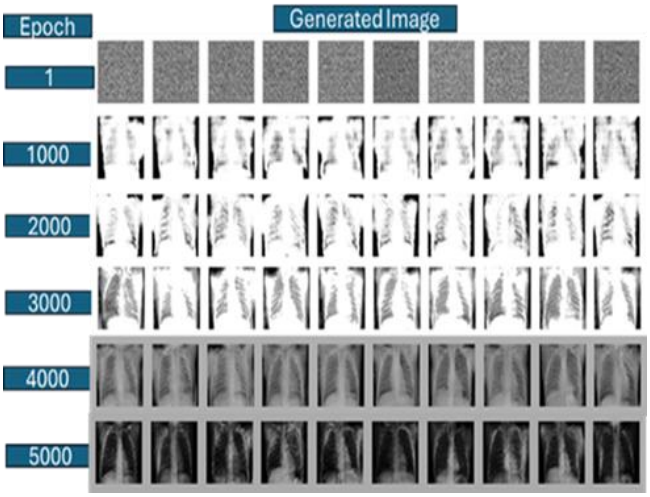

(c)

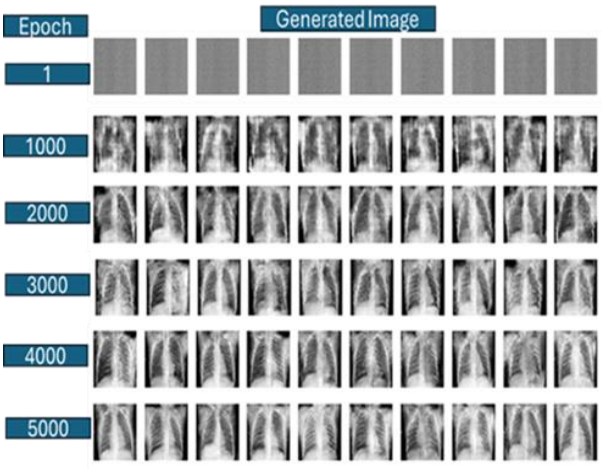

(c)

Fig. 3 Generation on Diabetic Retinopathy Dataset using (a) DCGAN (b) cGAN (c) CycleGAN (d) SRGAN

The figure presents the epoch-wise image generation performance for pneumonia chest X-ray images. In DCGAN (Fig. 4(a)), image clarity and structure improve steadily from epoch 1000 onwards, with sharper lung regions and clearer pathological features appearing by epoch 5000. cGAN (Fig. 4(b)), image clarity and structure improve steadily from epoch 2000 onwards. CycleGAN (Fig. 4(c)) also shows substantial progress after epoch 1000, successfully translating domain-specific features with well-formed lung structures and enhanced grayscale contrast by the later epoch. Conversely, SRGAN (Fig. 4(d)) struggles to generate meaningful outputs, with all epochs producing noisy, indistinct textures and failing to capture anatomical or pathological features of pneumonia, indicating poor convergence. DCGAN, cGAN and CycleGAN demonstrate effective pneumonia image generation with increasing training, while SRGAN underperforms in this medical imaging task.

Manuscript received February 8, 2024; Accepted April 25, 2025; date of publication May 8, 2025
Digital Object Identifier (**DOI**): https://doi.org/10.35882/jeeemi.v7i3.784

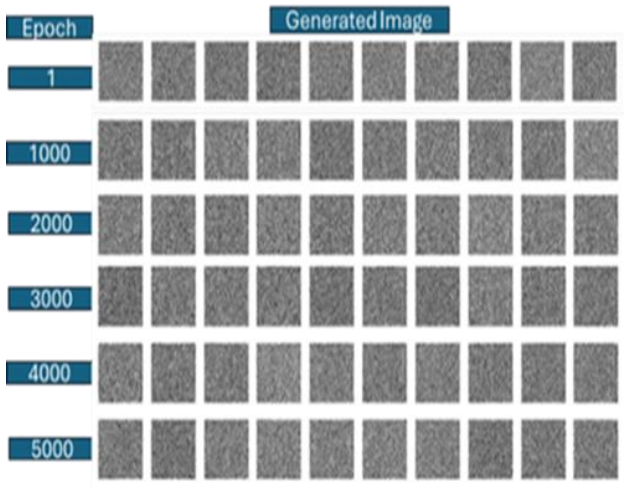

(d)

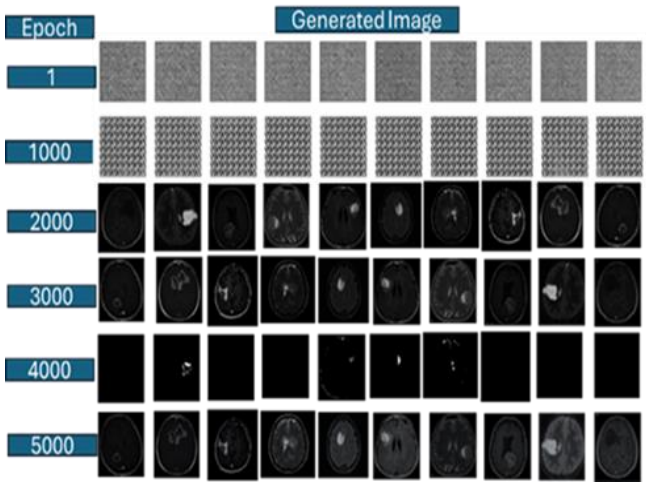

(e)

Fig. 4 Generation on Pneumonia Dataset using (a) DCGAN (b) cGAN (c) CycleGAN (d) SRGAN

The figure showcases brain tumor image generation. In DCGAN (Fig. 5(a)), early outputs are noisy, but by epoch 2000, distinct brain structures and tumor regions start emerging, with enhanced contrast and anatomical clarity by epoch 5000. cGAN (Fig. 5(b)), early outputs are noisy, but by epoch 3000, distinct brain structures and tumor regions start emerging, with enhanced contrast and anatomical clarity by epoch 5000. CycleGAN (Fig. 5(c)) exhibits similar behavior, progressing from repetitive patterns to realistic MRI-like tumor images, especially after epoch 3000, demonstrating its capacity for unpaired image-to-image translation. However, SRGAN (Fig. 5(d)) fails to converge, producing indistinct, noisy textures throughout all epochs without forming meaningful brain structures. Overall, DCGAN, cGAN and CycleGAN effectively synthesize brain tumor images over time, while SRGAN struggles with medical image realism in this context.

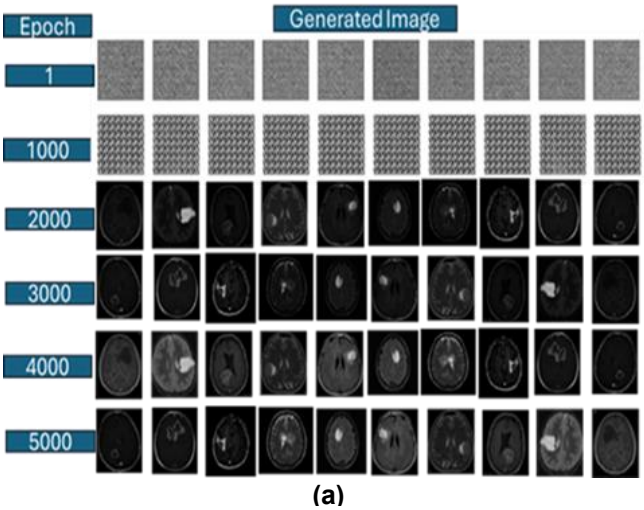

(a)

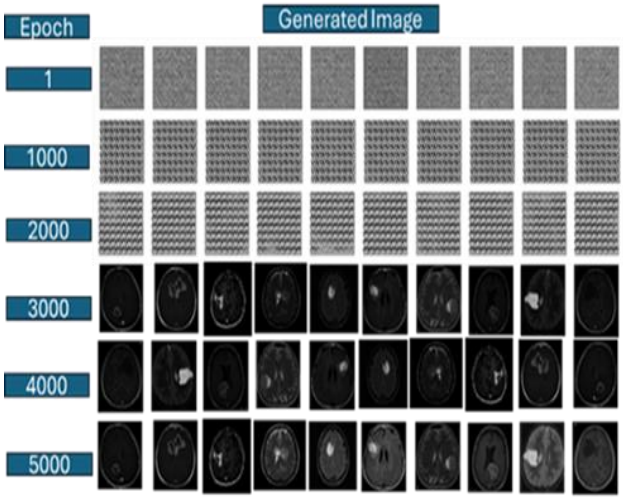

(c)

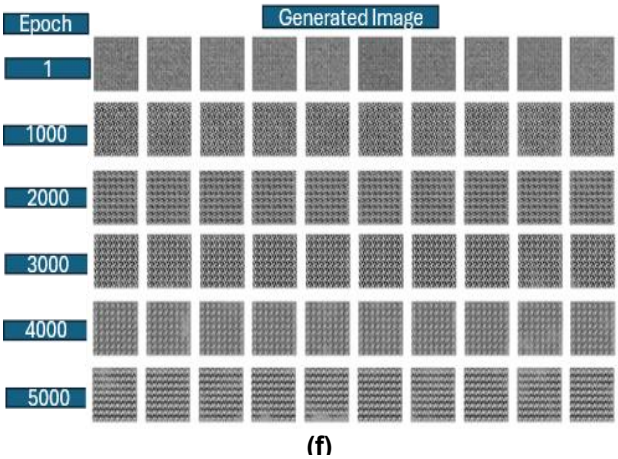

(f)

Fig. 5 Generation on Brain Tumor Dataset using (a) DCGAN (b) cGAN (c) CycleGAN (d) SRGAN

The figure illustrates the generation of skin cancer images. In DCGAN (Fig. 6(a)), image quality

Manuscript received February 8, 2024; Accepted April 25, 2025; date of publication May 8, 2025
Digital Object Identifier (**DOI**): https://doi.org/10.35882/jeeemi.v7i3.784

progressively improves with clearer lesion structures, color textures, and skin patterns becoming prominent after epoch 3000, achieving realistic dermoscopic image synthesis by epoch 5000. cGAN (Fig. 6(b)), image quality progressively improves with clearer lesion structures, color textures, and skin patterns becoming prominent after epoch 4000, achieving realistic dermoscopic image synthesis by epoch 5000. CycleGAN (Fig. 6(c)), however, fails to converge meaningfully; initial outputs show patterned noise, and from epoch 4000 onward, the generator produces completely black images, indicating mode collapse. SRGAN (Fig. 6(d)) remains trapped in patterned noise throughout all epochs, lacking any sign of feature learning or structural convergence. Thus, DCGAN demonstrates superior capability in generating realistic skin cancer images, while CycleGAN and SRGAN underperform significantly in this task.

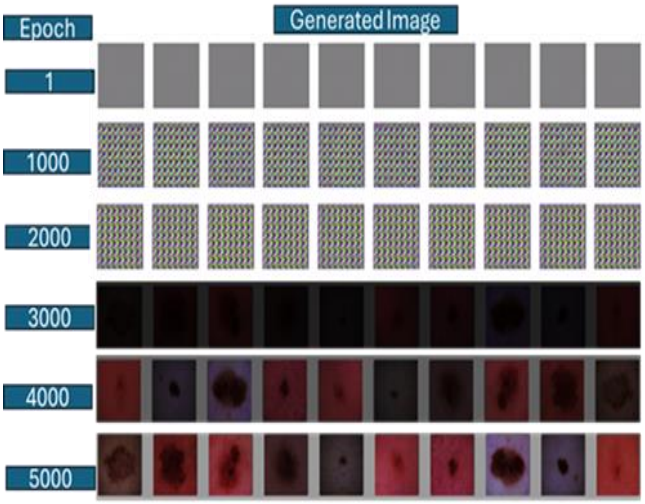

(a)

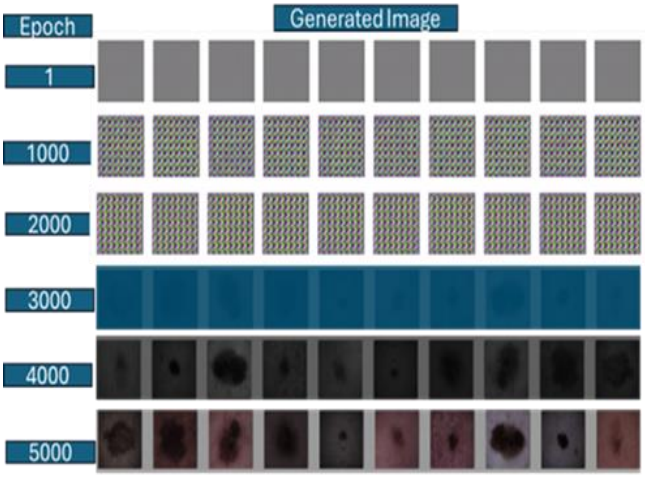

(g)

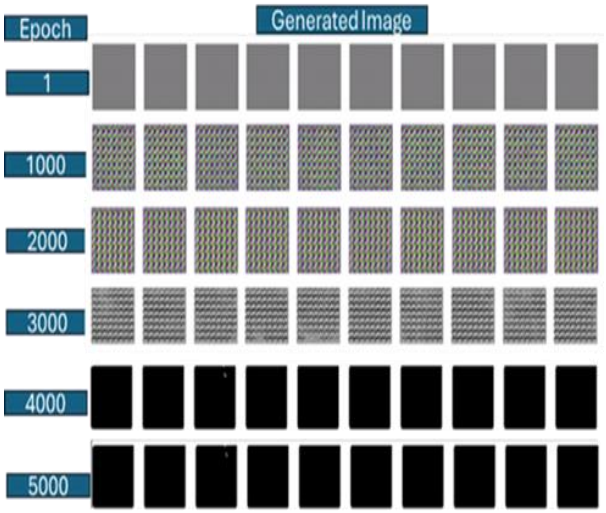

(c)

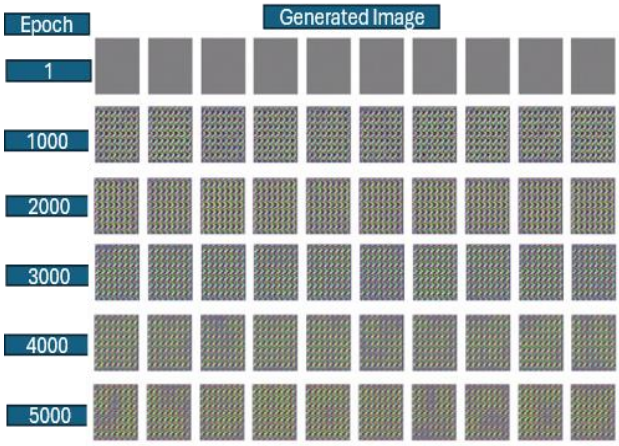

(h)

Fig. 6 Generation on Skin Cancer Dataset using (a) DCGAN (b) cGAN (c) CycleGAN (d) SRGAN

The figure displays leukemia cancer image synthesis using DCGAN, CycleGAN, and SRGAN across training epochs. DCGAN (Fig. 7(a)) shows early improvement with noise-to-patterned color transitions, and from epoch 3000, it begins forming cellular structures with improved color distribution and visual complexity by epoch 5000. cGAN (Fig. 7(b)) shows early improvement with noise-to-patterned color transitions, and from epoch 3000, it begins forming cellular structures with improved color distribution and visual complexity by epoch 5000. CycleGAN (Fig. 7(c)) follows a similar path up to epoch 4000 but then deteriorates into high-contrast black-and-white artifacts by epochs 4000–5000, indicating instability and loss of learned features. SRGAN (Fig. 7(d)), in contrast, exhibits repetitive and uninformative noisy outputs across all epochs, failing to model leukemia-specific visual features. Overall, DCGAN achieves moderate

Manuscript received February 8, 2024; Accepted April 25, 2025; date of publication May 8, 2025
Digital Object Identifier (**DOI**): https://doi.org/10.35882/jeeemi.v7i3.784

success in simulating leukemia cell image features, whereas CycleGAN suffers from instability and SRGAN lacks effective learning.

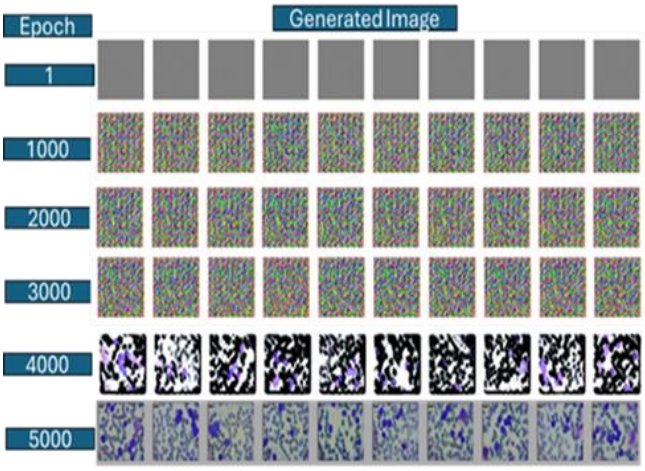

(a)

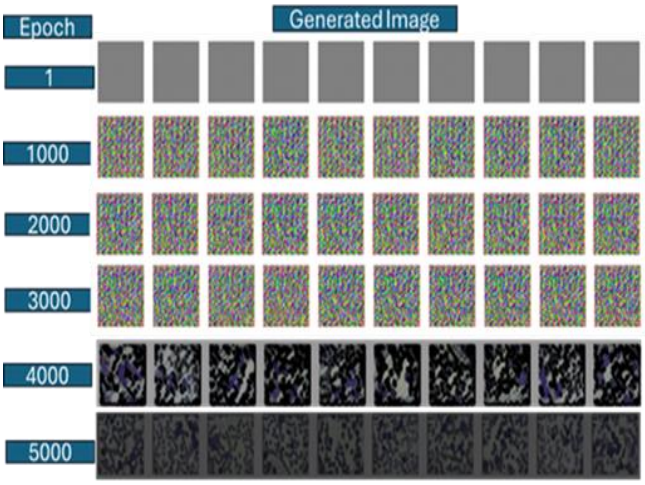

(i)

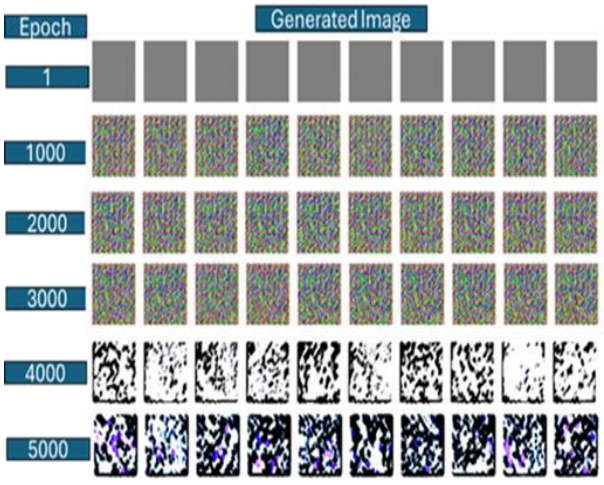

(c)

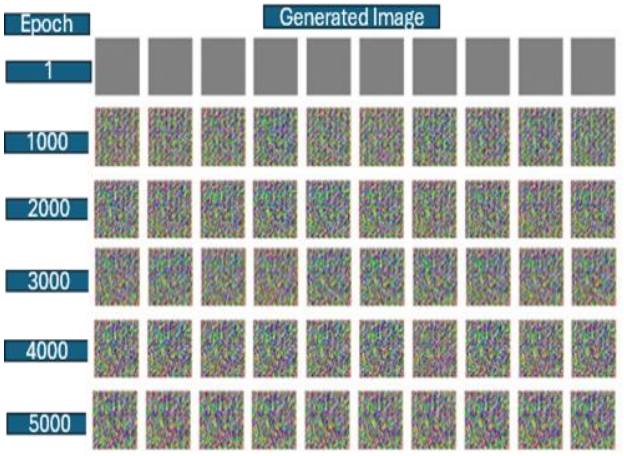

(j)

Fig. 7 Generation on Leukemia Cancer Dataset using (a) DCGAN (b) cGAN (c) CycleGAN (d) SRGAN

The loss performance of G and D was measured in Table 2 across five medical datasets through four GAN implementations, including DCGAN, cGAN, CycleGAN, and SRGAN. The five medical imaging datasets are Diabetic Retinopathy, Leukemia, Skin Cancer, Brain Tumor and Pneumonia. The CycleGAN model maintains lower loss values consistently across evaluations of the Diabetic Retinopathy and Leukemia datasets, making it more stable and offering better convergence than other analyzed models. The medical image generation benefits significantly from the increased stability delivered by this method. Neutral networks identify the SRGAN model as having top-notch resolution capabilities that led to successful outcomes, especially when analyzing the Skin Cancer dataset, which requires high-quality image inputs. SRGAN produces high-resolution images effectively yet slows down processing times because of its intricate design structure. The loss values of cGAN remained balanced throughout all datasets, thus proving its usefulness in diverse medical imaging applications.

Table 3 demonstrates an analytical breakdown of GAN architectures DCGAN, cGAN, CycleGAN, and SRGAN as they operate on five medical imaging datasets comprising Diabetic Retinopathy, Pneumonia, Brain Tumor, Skin Cancer, and Leukemia Cancer. According to the provided table, each GAN model requires a specified training duration and a specific number of parameters when working on these datasets. CycleGAN and SRGAN need longer training and extra parameters because they execute complex image translation operations. The training process of DCGAN runs quicker while using fewer parameters, but cGAN training times increase moderately, and its parameter usage exceeds DCGAN parameters.

Manuscript received February 8, 2024; Accepted April 25, 2025; date of publication May 8, 2025
Digital Object Identifier (**DOI**): https://doi.org/10.35882/jeeemi.v7i3.784

Table 2 Comparative Analysis of GANs

Different Medical Datasets	DCGAN		cGAN		CycleGAN		SRGAN	
	G Loss	D Loss	G Loss	D Loss	G Loss	D Loss	G Loss	D Loss
Diabetic Retinopathy	4.807	4.46	4.612	4.42	2.403	2.02	4.63	4.09
Pneumonia	0.59	0.29	0.52	0.22	0.69	0.38	0.7	0.4
Brain Tumor	0.78	0.47	0.76	0.45	1.2	0.65	1.42	0.82
Skin Cancer	6.24	6.25	6.22	6.21	4.211	4.124	6.253	6.119
Leukemia Cancer	5.564	5.36	5.231	5.234	3.325	3.129	5.232	5.102

Table 3 Computational Analysis of GANs

Different Medical Datasets	DCGAN		cGAN		CycleGAN		SRGAN	
	Time	Parameters	Time	Parameters	Time	Parameters	Time	Parameters
Diabetic Retinopathy	5hr	1.2M	6hr	1.5M	7hr	1.8M	8hr	2.1M
Pneumonia	4hr	0.9M	5hr	1.1M	6hr	1.4M	7hr	1.7M
Brain Tumor	6hr	1.3M	7hr	1.6M	8hr	1.9M	9hr	2.2M
Skin Cancer	7hr	1.4M	8hr	1.7M	9hr	2.0M	10hr	2.3M
Leukemia Cancer	6hr	1.2M	7hr	1.5M	8hr	1.7M	9hr	2.0M

**hr=Hour, M=Millions*

5. Discussion

A. GANs

This study aims to evaluates the performance of four GAN architectures—DCGAN, cGAN, CycleGAN, and SRGAN—across five distinct medical imaging datasets: Diabetic Retinopathy, Pneumonia, Brain Tumor, Skin Cancer, and Leukemia. These datasets represent diverse medical conditions, highlighting the importance of selecting the appropriate GAN architecture for each dataset's unique characteristics. The aim was to assess how these models handle the challenges posed by various medical image modalities.

Table 4 presents a comparative summary of studies using different GAN architectures for medical image generation. It shows the work done by various authors, the datasets used, the GAN types implemented, and the nature of each dataset. For instance, Wang et al. [1] focused on synthetic medical image generation using DCGAN and cGAN, with a focus on clinical imaging settings. Similarly, Chen et al. [3] utilized CycleGAN to generate medical images specifically for liver disease, while Sai Akhil et al. [7] applied DCGAN to chest X-ray images for synthesis. Nandal et al. [12] explored ESRGAN for super-resolution in medical images, while Jha & lima [14] used CycleGAN for cross-modality synthesis (CT to MRI). The dataset characteristics in these studies are diverse, with some focusing on specific medical conditions, such as liver disease or chest X-rays, while others for super-resolution or cross-modality generation. While proposed study importance of a multi-disease dataset and diverse GANs, which aims to generate synthetic medical images

B. Model Performance

The results in Fig. 2-6 and Table 2 show that DCGAN consistently produces stable and high-quality synthetic images, as reflected by its lower generator and discriminator losses compared to other models. Within 5 hours of training, the DCGAN generated images with a loss value of 4.807 for the generators and 4.46 for the discriminators when utilizing an architectural model containing 1.2M parameters in the Diabetic Retinopathy dataset. The findings match Wang et al. [1] because DCGAN demonstrates efficient image

Manuscript received February 8, 2024; Accepted April 25, 2025; date of publication May 8, 2025
Digital Object Identifier (**DOI**): https://doi.org/10.35882/jeeemi.v7i3.784

Table 4 Comparative Analysis with Existing Research

Work Done	Used Datasets	GAN Types	Dataset Characteristics
Wang et al. [1]	Synthetic Medical Image Generation	DCGAN, cGAN	Focus on medical imaging in clinical settings
Chen et al. [3]	Liver Medical Images	CycleGAN	Medical images focused on liver disease
Sai Akhil et al. [7]	Chest X-Ray Images	DCGAN	Medical imaging for chest X-ray synthesis
Nandal et al. [12]	Medical Images	ESRGAN	Super-resolution of medical images
Jha & Iima [14]	CT & MRI Images	CycleGAN	Cross-modality synthesis (CT to MRI)
Proposed Work	Diabetic Retinopathy, Pneumonia, Brain Tumor, Skin Cancer, Leukemia Cancer	DCGAN, cGAN, CycleGAN, SRGAN	Multi-disease dataset, diverse GANs for different medical imaging tasks

production together with quick training sessions, which produce both high image quality and fast training times.

The generator losses in Diabetic Retinopathy (2.403) and Leukemia (3.325) decreased when using CycleGAN, yet the model exhibited unstable behavior that matched Chen et al. [3] findings from liver disease datasets. cGAN operated stably across all datasets, yet its loss value exceeded DCGAN's ranges, as reported by Sai Akhil et al. [7] with chest X-ray images. The SRGAN failed to maintain critical clinical characteristics from grayscale images in Pneumonia and Brain Tumor datasets, thus reducing diagnostic accuracy. The same synthetic cross-modality impediment persists, according to the findings of Jha & Iima [14]. DCGAN achieved superior efficiency compared to the other models according to loss measurements and training time assessments (Table 3). CycleGAN maintained lower generator loss points at some point; however, it became less stable as training time stretched too long. High-resolution images from SRGAN remain a strong point of the model, but the model struggles to safeguard clinical characteristics visible in grayscale medical pictures. Data from different datasets demonstrates that DCGAN gives the best training effectiveness and image quality stability for medical image generation. The research findings agree with Wang et al. [1], Chen et al. [3] and Sai Akhil et al. [7] and Jha & Iima [14] regarding GAN architecture strengths and weaknesses for medical image generation.

6. Conclusion

This study aims to develop a synthetic medical image generator using DCGAN, cGAN, CycleGAN, and SRGAN across five medical datasets: diabetic retinopathy, pneumonia, brain tumor, skin cancer, and leukemia. The results showed that the DCGAN algorithm outperformed other models regarding generator and discriminator loss across most datasets, producing more stable and high-quality synthetic images. For example, DCGAN achieved the lowest loss values for diabetic retinopathy (G Loss: 4.807, D Loss: 4.46) and skin cancer (G Loss: 6.24, D Loss: 6.25), while CycleGAN and SRGAN exhibited higher loss values, particularly in more complex datasets such as brain tumor and leukemia. Although cGAN showed comparable performance in simpler datasets like pneumonia, it lacked consistency in diverse imaging modalities. Additionally, DCGAN demonstrated superior computational efficiency by requiring the least training time and parameter count across all datasets. For instance, it generated pneumonia images in 4 hours using only 0.9 million parameters, compared to SRGAN, which needed 7 hours and 1.7 million parameters. The proposed DCGAN framework balances image quality and computational efficiency, maintaining training durations and resource consumption within acceptable thresholds. This makes it suitable for practical deployment in medical imaging workflows. Moving forward, future research should investigate integrating attention mechanisms and hybrid GAN architectures to improve further the clinical realism and diagnostic relevance of synthetic medical images across diverse imaging modalities and tasks.

References

[1] J. Wang et al., “Self-improving generative foundation model for synthetic medical image generation and clinical applications,” Nature Medicine, vol. 31, no. 2, pp. 609–617, 2025.

[2] M. Kumar, A. S. Chivukula, and G. Barua, “Deep learning-based encryption scheme for medical images using DCGAN and virtual planet domain,” Scientific Reports, vol. 15, no. 1, p. 1211, 2025, doi: 10.1038/s41598-024-84186-6.

Manuscript received February 8, 2024; Accepted April 25, 2025; date of publication May 8, 2025
Digital Object Identifier (**DOI**): https://doi.org/10.35882/jeeemi.v7i3.784

[3] Y. Chen et al., "ICycle-GAN: Improved cycle generative adversarial networks for liver medical image generation," Biomedical Signal Processing and Control, vol. 92, p. 106100, 2024, doi: 10.1016/j.bspc.2024.106100.

[4] M. Ali, M. Ali, M. Hussain, and D. Koundal, "Generative Adversarial Networks (GANs) for Medical Image Processing: Recent Advancements," Archives of Computational Methods in Engineering, pp. 1–14, 2024, doi: 10.1007/s11831-024-10174-8.

[5] M. K. Sherwani and S. Gopalakrishnan, "A systematic literature review: deep learning techniques for synthetic medical image generation and their applications in radiotherapy," Frontiers in Radiology, vol. 4, p. 1385742, 2024, doi: 10.3389/fradi.2024.1385742.

[6] M. Hamghalam and A. L. Simpson, "Medical image synthesis via conditional GANs: Application to segmenting brain tumours," Computers in Biology and Medicine, vol. 170, p. 107982, 2024, doi: 10.1016/j.compbiomed.2024.107982.

[7] M. C. Sai Akhil, B. S. Sanjana Sharma, A. Kodipalli, and T. Rao, "Medical Image Synthesis Using DCGAN for Chest X-Ray Images," in 2024 International Conference on Knowledge Engineering and Communication Systems, ICKECS 2024, 2024, vol. 1, pp. 1–8. doi: 10.1109/ICKECS61492.2024.10617031.

[8] R. Zakaria, H. Abedlamjid, D. Zitouni, and A. Elqaraoui, "Medical-DCGAN: Deep Convolutional GAN for Medical Imaging," in Advances in Emerging Financial Technology and Digital Money, CRC Press, 2024, pp. 123–134. doi: 10.1201/9781032667478-10.

[9] D. Shah, M. A. Ullah Khan, and M. Abrar, "Reliable Breast Cancer Diagnosis with Deep Learning: DCGAN-Driven Mammogram Synthesis and Validity Assessment," Applied Computational Intelligence and Soft Computing, vol. 2024, no. 1, p. 1122109, 2024, doi: 10.1155/2024/1122109.

[10] S. Varshitha, N. Lavanya, M. Shirisha, S. Manmatti, K. P. Asha Rani, and S. Gowrishankar, "Enhancing Medical Imaging Resolution: Exploring SRGAN for High-Quality Medical Image Reconstruction," in Proceedings of ICWITE 2024: IEEE International Conference for Women in Innovation, Technology and Entrepreneurship, 2024, pp. 1–8. doi: 10.1109/ICWITE59797.2024.10503215.

[11] S. Madhav, T. M. Nandhika, and M. K. Kavitha Devi, "Super Resolution of Medical Images Using SRGAN," in 2nd International Conference on Emerging Trends in Information Technology and Engineering, ic-ETITE 2024, 2024, pp. 1–6. doi: 10.1109/ic-ETITE58242.2024.10493588.

[12] P. Nandal, S. Pahal, A. Khanna, and P. R. Pinheiro, "Super-resolution of medical images using real ESRGAN," IEEE Access, 2024, doi: 10.1109/ACCESS.2024.3497002.

[13] Y. Heng, M. Yinghua, F. G. Khan, A. Khan, and Z. Hui, "HLSNC-GAN: Medical Image Synthesis Using Hinge Loss and Switchable Normalization in CycleGAN," IEEE Access, vol. 12, pp. 55448–55464, 2024, doi: 10.1109/ACCESS.2024.3390245.

[14] A. Jha and H. Iima, "CT to MRI Image Translation Using CycleGAN: A Deep Learning Approach for Cross-Modality Medical Imaging," in International Conference on Agents and Artificial Intelligence, 2024, vol. 3, pp. 951–957. doi: 10.5220/0012422900003636.

[15] K. Afnaan, T. Singh, and P. Duraisamy, "Hybrid Deep Learning Framework for Bidirectional Medical Image Synthesis," in 2024 15th International Conference on Computing Communication and Networking Technologies, ICCCNT 2024, 2024, pp. 1–6. doi: 10.1109/ICCCNT61001.2024.10725975.

[16] R. Raad et al., "Conditional generative learning for medical image imputation," Scientific Reports, vol. 14, no. 1, p. 171, 2024, doi: 10.1038/s41598-023-50566-7.

[17] R. Wang, A. F. Heimann, M. Tannast, and G. Zheng, "CycleSGAN: A cycle-consistent and semantics-preserving generative adversarial network for unpaired MR-to-CT image synthesis," Computerized Medical Imaging and Graphics, vol. 117, p. 102431, 2024, doi: 10.1016/j.compmedimag.2024.102431.

[18] M. U. Akbar, W. Wang, and A. Eklund, "Beware of diffusion models for synthesizing medical images -- A comparison with GANs in terms of memorizing brain MRI and chest x-ray images," Machine Learning: Science and Technology, vol. 6, no. 1, p. 15022, 2023, doi: 10.1088/2632-2153/ad9a3a.

[19] Y. S. Devi and S. Phani Kumar, "Diabetic Retinopathy (DR) Image Synthesis Using DCGAN and Classification of DR Using Transfer Learning Approaches," International Journal of Image and Graphics, vol. 24, no. 05, p. 2340009, 2023, doi: 10.1142/S0219467823400090.

[20] A. A. Mamo, B. G. Gebresilassie, A. Mukherjee, V. Hassija, and V. Chamola, "Advancing Medical Imaging Through Generative Adversarial Networks: A Comprehensive Review and Future

Manuscript received February 8, 2024; Accepted April 25, 2025; date of publication May 8, 2025
Digital Object Identifier (**DOI**): https://doi.org/10.35882/jeeemi.v7i3.784

Prospects," Cognitive Computation, vol. 16, no. 5, pp. 2131–2153, 2024, doi: 10.1007/s12559-024-10291-3.

[21] P. Friedrich, Y. Frisch, and P. C. Cattin, "Deep Generative Models for 3D Medical Image Synthesis," in Generative Machine Learning Models in Medical Image Computing, Springer, 2024, pp. 255–278. [Online]. Available: http://arxiv.org/abs/2410.17664

[22] A. S. Fard, D. C. Reutens, S. C. Ramsay, S. J. Goodman, S. Ghosh, and V. Vegh, "Image synthesis of interictal SPECT from MRI and PET using machine learning," Frontiers in Neurology , vol. 15, p. 1383773, 2024, doi: 10.3389/fneur.2024.1383773.

[23] S. Islam et al., "Generative Adversarial Networks (GANs) in Medical Imaging: Advancements, Applications, and Challenges," IEEE Access, vol. 12, pp. 35728–35753, 2024, doi: 10.1109/ACCESS.2024.3370848.

[24] D. N. Sindhura, R. M. Pai, S. N. Bhat, and M. M. M. Pai, "A review of deep learning and Generative Adversarial Networks applications in medical image analysis," Multimedia Systems, vol. 30, no. 3, p. 161, 2024, doi: 10.1007/s00530-024-01349-1.

[25] D. S. Kermany et al., "Identifying Medical Diagnoses and Treatable Diseases by Image-Based Deep Learning," Cell, vol. 172, no. 5, pp. 1122-1131.e9, Feb. 2018, doi: 10.1016/j.cell.2018.02.010.

[26] P. Mooney, "Chest X-ray images (Pneumonia)," Kaggle, 2018. Available: https://www.kaggle.com/datasets/paultimothymooney/chest-xray-pneumonia. Accessed: Feb. 9, 2024.

[27] E. Dugas, Jared, Jorge, and W. Cukierski, "Diabetic retinopathy detection," Kaggle, 2015. Available: https://kaggle.com/competitions/diabetic-retinopathy-detection. Accessed: Feb. 9, 2024.

[28] N. Paul, "Brain MRI images for brain tumor detection," Kaggle, 2019. Available: https://www.kaggle.com/datasets/navoneel/brain-mri-images-for-brain-tumor-detection. Accessed: Apr. 21, 2025.

[29] A. Fanconi, "Skin cancer: Malignant vs. benign," Kaggle, 2021. Available: https://www.kaggle.com/datasets/fanconic/skin-cancer-malignant-vs-benign. Accessed: Apr. 21, 2025.

[30] V. Tanwar, "Leukemia cancer small dataset," Kaggle, 2022. Available: https://www.kaggle.com/datasets/visheshtanwar26/leukemia-cancer-small-dataset/data. Accessed: Apr. 21, 2025.

Author Biography

Shrina Patel is currently serving as an Assistant Professor at SVIT Vasad, Gujarat, India, and is pursuing her Ph.D. at CHARUSAT University. She holds a strong academic background in Computer Engineering Department and has over several years of experience in teaching, mentoring, and academic administration. Her areas of interest include Artificial Intelligence, Machine Learning, Data Mining, Image Processing, Computer Vision and Text Processing. She emphasizes outcome-based education, project-based learning, and skill enhancement. She has contributed to reputed journals, conferences, and book chapters. As a committed academician, she is passionate about student development, research innovation, knowledge dissemination, and contributing to institutional excellence.

Dr. Ashwin Makwana is an Associate Professor in the U & P U Patel Department of Computer Engineering at CHARUSAT University, Gujarat, India. He also leads the Career Development and Placement Cell and the Human Resource Development Center. Holding a Ph.D. in Computer Engineering with specialization in Artificial Intelligence, he brings over 19 years of academic and professional experience. His core areas of expertise include Artificial Intelligence, Machine Learning, Semantic Web technologies, Software Engineering, and Project Management. Dr. Makwana has authored and presented numerous research papers at reputed national and international platforms and actively contributes to curriculum innovation, industry collaboration, and academic leadership.

Manuscript received February 8, 2024; Accepted April 25, 2025; date of publication May 8, 2025
Digital Object Identifier (**DOI**): https://doi.org/10.35882/jeeemi.v7i3.784